

AperTO - Archivio Istituzionale Open Access dell'Università di Torino

## Microwave-induced crystallization of AC/TiO<sub>2</sub> for improving the performance of rhodamine B dye degradation

### This is the author's manuscript

*Original Citation:*

*Availability:*

This version is available <http://hdl.handle.net/2318/1576938> since 2016-06-30T22:38:35Z

*Published version:*

DOI:10.1016/j.apsusc.2015.05.133

*Terms of use:*

Open Access

Anyone can freely access the full text of works made available as "Open Access". Works made available under a Creative Commons license can be used according to the terms and conditions of said license. Use of all other works requires consent of the right holder (author or publisher) if not exempted from copyright protection by the applicable law.

(Article begins on next page)

This Accepted Author Manuscript (AAM) is copyrighted and published by Elsevier. It is posted here by agreement between Elsevier and the University of Turin. Changes resulting from the publishing process - such as editing, corrections, structural formatting, and other quality control mechanisms - may not be reflected in this version of the text. The definitive version of the text was subsequently published in APPLIED SURFACE SCIENCE, 351, 2015, 10.1016/j.apsusc.2015.05.133.

You may download, copy and otherwise use the AAM for non-commercial purposes provided that your license is limited by the following restrictions:

- (1) You may use this AAM for non-commercial purposes only under the terms of the CC-BY-NC-ND license.
- (2) The integrity of the work and identification of the author, copyright owner, and publisher must be preserved in any copy.
- (3) You must attribute this AAM in the following format: Creative Commons BY-NC-ND license (<http://creativecommons.org/licenses/by-nc-nd/4.0/deed.en>), 10.1016/j.apsusc.2015.05.133

The publisher's version is available at:

<http://linkinghub.elsevier.com/retrieve/pii/S0169433215012611>

When citing, please refer to the published version.

Link to this full text:

<http://hdl.handle.net/2318/1576938>

# Microwave-induced crystallization of AC/TiO<sub>2</sub> for improving the performance of Rhodamine B dye degradation

Fei Tian<sup>a</sup>, Zhansheng Wu<sup>a,\*</sup>, Qiuyu Chen<sup>a</sup>, Yujun Yan<sup>a</sup>, Giancarlo Cravotto<sup>b</sup>, Zhilin Wu<sup>b</sup>

<sup>a</sup>School of Chemistry and Chemical Engineering, Shihezi University, Shihezi 832003, PR China

<sup>b</sup>Dipartimento di Scienza e Tecnologia del Farmaco, University of Turin, Torino 10125, Italy

Titanium dioxide (TiO<sub>2</sub>) deposition on activated carbon (AC) is widely used for pollutant photodegradation. In this study, a simple and efficient method for preparing AC/TiO<sub>2</sub> composites under microwave irradiation was developed for photocatalytic degradation of Rhodamine B (RhB) under UV light. Results of X-ray diffraction, scanning electron microscopy, and transmission electron microscopy revealed that TiO<sub>2</sub> nanoparticles are anatase and rutile, with a spherical shape and a particle size of 20–50 nm and are well distributed on the AC surface. The UV-vis spectrum of TiO<sub>2</sub> coated on AC showed an evident red-shift and exhibited stronger optical absorption capacity than pure TiO<sub>2</sub>. The AC/TiO<sub>2</sub> nanoparticles prepared at a microwave power of 700 W for 15 min exhibited 98% efficiency in removing RhB dye under UV irradiation for 30 min. The high photocatalytic activity of AC/TiO<sub>2</sub>-700 W could be mainly attributed to the high sorption capacity of the mesoporous carbon material and high TiO<sub>2</sub> content, which could produce higher quantity of ·OH. This study provides a rapid synthesis technique to prepare AC/TiO<sub>2</sub> and a novel method to improve photocatalytic efficiency via synergistic effect for other catalytic systems.

**Keywords:** anatase-rutile; microwave irradiation; mesoporous carbon; photocatalysis; adsorption.

## 1. Introduction

Water pollution has become one of the most serious problems of our society. Organic poisonous contaminants including xanthene dyes are of the most harmful water pollutants.

Rhodamine B (RhB) is an important xanthene dye used as a laser and colorant for textile materials because of its good stability [1]. According to the International Agency for Research on Cancer, RhB may cause acute and chronic poisoning through ingestion, inhalation, and skin contact. This poisonous organic contaminant can be removed from water through various methods, such as chemical precipitation, advanced oxidation, electrochemical techniques, and ion exchange [2-5]. As applications of these methods are limited because of technical difficulties or environment hazards [6-7], an effective and optimal strategy to rapidly remove RhB from water and wastewater must be developed.

Semiconductor photocatalysts are the most cost-optimal, effective, and environment friendly material for applications directed toward energy and environmental concerns [8-10]. Among these photocatalysts, titanium dioxide ( $\text{TiO}_2$ ) is widely used in heterogeneous photocatalysis to degrade organic pollutants in water and air because it features nontoxicity, chemical and biological inertness, and low cost [11-16].  $\text{TiO}_2$  nanoparticles are generally synthesized through different methods, such as hydrothermal, sol-gel, and electrochemical [17-18]. These methods involve a conventional thermal treatment process using a high-temperature furnace for annealing [19-22]. Nevertheless, heating a furnace consumes a high amount of energy and time. In this regard, microwave-hydrothermal technique, as a novel and fast method, has attracted much interest in recent years [23]. Microwaves exhibit potential for various applications and the use of microwaves provides a fast heating process, thereby saving energy and money and shortening synthesis time [24, 25]. Chen et al. [26] reported that the reaction time for  $\text{TiO}_2$  crystallization decreased from 16 h via the hydrothermal process to 80 min via microwave irradiation.

In most of the cases, the degradation efficiency of  $\text{TiO}_2$  is relatively low in practical

application because of its small surface area and the poor adsorption of organic poisonous contaminants onto it [27, 28]. TiO<sub>2</sub> supported on activated carbon that provided the crystalline framework to support TiO<sub>2</sub> nanoparticles, has been adopted in removal of organic contaminants. Pastravanu et al. [29] synthesized TiO<sub>2</sub>-coated carbon samples that exhibited high photocatalytic activity, such that 92% of methyl orange (MO) was degraded after 170 min of UV irradiation. The studies showed that the microwave-assisted synthesis requires a shorter reaction time than conventional methods. Nevertheless, to the best of our knowledge, limited studies have used microwave radiation to synthesize AC/TiO<sub>2</sub> for rapid photocatalysis of RhB. Furthermore, no studies have reported the effects of microwave conditions on the properties of TiO<sub>2</sub> loaded on AC and on the catalytic performance of AC/TiO<sub>2</sub>.

In this study, AC/TiO<sub>2</sub> was synthesized via a simple, fast, and efficient one-step method under different microwave conditions. Brunauer–Emmett–Teller (BET) surface area, X-ray diffraction (XRD), scanning electron microscopy (SEM), transmission electron microscopy (TEM), X-ray photoelectron spectroscopy (XPS), Fourier-transform infrared (FTIR) spectroscopy, and UV-vis diffusion reflection spectroscopy (DRS) were utilized to assess the photocatalytic performance of the enhanced catalyst. In addition, photocatalytic degradation of RhB by AC/TiO<sub>2</sub> and bare TiO<sub>2</sub> was evaluated under different microwave powers.

## **2. Materials and methods**

### **2.1 Preparation of AC/TiO<sub>2</sub>**

AC was prepared based on our previous study [30]. It was using a microwave oven (MM823LA6-NS, Midea) at a frequency of 2.45 GHz. A mixture of solid KOH (10 g) and dried coal at a ratio of 1:1 was placed in a quartz tube in a microwave reactor and activated under

vacuum atmosphere at 693 W for 10 min. The KOH is intercalated to the carbon matrix responsible for both stabilization and widening of the spaces between the carbon atomic layers. Metallic potassium formed during redox reaction can be intercalated into the carbon walls independently of the structural order responsible for separation and degradation of graphitic layers thus develop the microporosity and mesoporosity. The obtained AC samples were pretreated by adding into HNO<sub>3</sub> solution with 24 h. The mixture was filtered using distilled water until they became neutral. The pretreated AC was then dried and stored until use.

The TiO<sub>2</sub> gel/sol was obtained by conventional sol-gel method. All reagents were of analytical grade and used without further purification. In typical synthesis process, 30 mL of tetrabutyl orthotitanate (TBOT) was dissolved in anhydrous alcohol (EtOH) in proportion of 1:1 (volume ratio). This solution was thoroughly stirred for 40 min and named solution A. Solution B was prepared by mixing 14 mL of glacial acetic acid and 7 mL of distilled water in 35 mL of absolute alcohol. Solution B was added to solution A dropwise and continuously stirred for 1 h. Then it was obtained pale yellow clear TiO<sub>2</sub> sol.

AC/TiO<sub>2</sub> nanoparticles were prepared as follows. Pretreated AC (10 g) was added into TiO<sub>2</sub> sol (100 g) [31]. The mixture was placed in an oven at 100 °C for 24 h. After solidification, AC/TiO<sub>2</sub> was prepared under different microwave conditions: irradiation at 100 W for 30 min or at 300–900 W for 15 min based on results of preliminary experiment, the microwave oven followed a working cycle of 6 s on and 24 s off (20% power). The resulted samples were noted as AC/TiO<sub>2</sub>-100 W, AC/TiO<sub>2</sub>-300 W, AC/TiO<sub>2</sub>-500 W, AC/TiO<sub>2</sub>-700 W and AC/TiO<sub>2</sub>-900 W.

## **2.2 Catalyst characterization**

The prepared samples were characterized through XRD on a Rigaku D/Max-2500/PC powder

diffractometer. Each sample powder was scanned using Cu- $K\alpha$  radiation with an operating voltage of 40 kV and an operating current of 200 mA. The scan rate of 5°/min was applied to record the patterns in the range of 10-80° at a step of 0.02°. XPS analysis of samples was conducted using a PHI5700 ESCA system equipped with a Mg  $K\alpha$  X-ray source (1253.6 eV) under a vacuum pressure  $<10^{-6}$  Pa. Pass energy was set as 187.85 and 29.35 eV for the survey and high-resolution spectra, respectively. The XPS spectra of the samples were calibrated by taking the graphitic carbon peak as 284.6 eV. The surface micromorphologies of AC and AC/TiO<sub>2</sub> were characterized through SEM (S4800, Hitachi LTD) at an accelerating voltage of 15 kV. TEM was performed on a Tecnai G2 F20 microscope at 100 kV. FTIR spectra were recorded with a Bruker Vertex FTIR spectrometer, resolution of 2 cm<sup>-1</sup>, in the range of 4000-400 cm<sup>-1</sup> by KBr pellet technique. The UV-vis DRS were obtained with a powder UV-vis spectrophotometer (U-4100, Hitachi LTD). Specific surface area (SBET, m<sup>2</sup>·g<sup>-1</sup>) was calculated using the BET equation, and total pore volume ( $V_t$ , m<sup>3</sup>·g<sup>-1</sup>) was evaluated by converting the adsorption amount at  $P/P_0 = 0.95$  to the volume of liquid adsorbate. Micropore volume, micropore surface area, and external surface area were determined using t-plot method. Average pore size ( $r$ , Å) was estimated with the following equation:

$$r = \frac{4V_t}{SBET} \quad (2-1)$$

The formation rate of ·OH at photo-illuminated sample/water interface was detected by the Photoluminescence (PL) technique using terephthalic acid (TA) as a probe molecule. PL spectroscopy of synthesized products was taken at room temperature on a Hitachi F2500 spectrofluorometer using a Xe lamp with an excitation wavelength of 325 nm.

### 2.3 Photocatalytic activity for RhB degradation

Photocatalytic experiments were performed to investigate UV-assisted degradation of RhB solution by AC/TiO<sub>2</sub> at room temperature by using a 1000 W UV lamp with 365 nm wavelength. In a typical test, 0.01 g of catalyst was added to 50 mL of RhB solution (30 mg/L, pH=6.8). The mixture was kept in the dark for 30 min to allow adsorption of RhB on the AC/TiO<sub>2</sub> surface. The mixture was then irradiated under UV lamp to degrade RhB. The distance between the reactor and lamp housing is 8.5 cm.

The removal rate ( $\eta$ ) of RhB can be calculated as follows:

$$\eta = \frac{C_o - C_t}{C_o} \times 100 \quad (2-2)$$

where  $C_o$  and  $C_t$  are the concentrations of RhB at initial and different irradiation times, respectively.

### 3. Results and discussion

#### 3.1 XRD spectra

[Fig. 1](#) depicts the XRD patterns of neat AC as support and AC/TiO<sub>2</sub>. No diffraction patterns from carbon species were detected in all samples. All AC/TiO<sub>2</sub> composites exhibited peaks at  $2\theta = 25.281^\circ$ , which is a characteristic of the anatase phase (101). The average crystallite sizes of the anatase and rutile phase calculated from the Scherrer equation are listed in Table 1. The calculated crystal sizes of the samples range from 10 nm to 50 nm. These results indicated that TiO<sub>2</sub> loaded on the AC powder are nanoparticles.

[Fig. 1](#) shows that after 100 W of microwave radiation, the XRD peaks of the TiO<sub>2</sub> anatase phase could be detected in the powder sample without other phase. When the microwave power was increased, the mixed crystals of anatase [JCDPS No. 21-1272] and rutile [JCDPS No. 21-1276] [11] were observed ([Fig. 1 \(b\)-\(e\)](#)). The anatase to rutile phase transformation is generally



considered as nucleation growth process during which the rutile nuclei are formed within the anatase phase [4]. Thus, various crystallite size of anatase can be obtained in the formation process of rutile under different prepared condition. With an increase of the microwave power from 300 W to 900 W, the content of rutile increased see in Table 1. As the energy position of the anatase conduction band edge is higher than that of rutile, the photogenerated electrons migrate from anatase to rutile and the positive holes migrate from rutile to anatase. Hence, low electron–hole recombination can enhance the photocatalytic activity of the mixed-phase  $\text{TiO}_2$ . When the microwave power was increased, the degree of crystallinity in the structural order also increased (narrower peaks) [8], while no further improvement was observed at power exceeding 700 W. As photoreactivity requires a balance among crystallinity, specific surface area, and porosity, we prepared amorphous  $\text{TiO}_2$  gel through fast microwave crystallization and improved the crystallinity of  $\text{TiO}_2$  spheres with minimal loss in the SBET and porosity. Compared with as-synthesized  $\text{TiO}_2$  (for 700 W with 15 min), AC/ $\text{TiO}_2$ -700 W show the same peaks. Thus, combination with AC does not influence the crystal structure of the host  $\text{TiO}_2$  material. The XRD results demonstrated that microwave is a promising synthesis technique to enhance the crystallinity of AC/ $\text{TiO}_2$ .

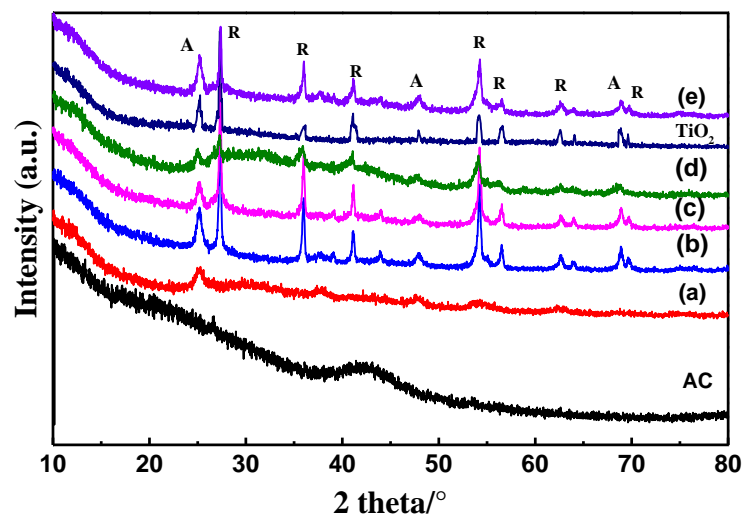


Fig. 1 XRD patterns of AC,  $\text{TiO}_2$  (for 700 W with 15 min) and AC/ $\text{TiO}_2$ : (a) AC/ $\text{TiO}_2$ -100 W, (b)

AC/TiO<sub>2</sub>-300 W, (c) AC/TiO<sub>2</sub>-500 W, (d) AC/TiO<sub>2</sub>-700 W, (e) AC/TiO<sub>2</sub>-900 W. A: anatase crystalline phase of TiO<sub>2</sub> and R: rutile crystalline phase of TiO<sub>2</sub>.

### 3.2 BET

Surface areas and pore size distribution of the samples were determined through N<sub>2</sub> sorption measurements. SBET,  $V_t$ , and mean pore diameter ( $d_{\text{mean}}$ ) obtained from N<sub>2</sub> adsorption/desorption measurements are presented in Table 1. Pure AC presented large SBET and  $V_t$ , whereas AC/TiO<sub>2</sub> demonstrated decreased SBET of more than 50% and decreased  $V_t$ . This phenomenon could be due to the generated TiO<sub>2</sub> crystals and other solid matter that covered the AC surface and blocked the pore structure. The BET surface of AC/TiO<sub>2</sub> evidently increased when the microwave power increased from 100 to 700 W. This phenomenon is probably due to sublimation of the covered solid matter which reduced the blocked surface of AC, thereby increasing the exposed surface area. When the microwave power was increased to 900 W, the SBET of AC/TiO<sub>2</sub> decreased because the reunion of titanium dioxide crystals and collapse of the AC structure induced by high temperatures.

Fig. 2 shows the N<sub>2</sub> adsorption–desorption isotherms of uncoated and TiO<sub>2</sub>-coated AC and the pore size distribution (inset) calculated by BJH method. A unimodal distribution centralized at 3.8 nm was observed in AC and AC/TiO<sub>2</sub> (300–900 W) powders, whereas AC/TiO<sub>2</sub>-100 W showed very small mesopores of approximately 3.414 nm. This characteristic could be due to incomplete crystal formation of TiO<sub>2</sub> sol at a low microwave power (100 W). Although AC and AC/TiO<sub>2</sub> showed similar peaks, the latter presented significantly lower intensity, indicating that the carbon pore entrance was blocked by TiO<sub>2</sub> nanoparticles. Data on average pore diameter indicated that all prepared photocatalysts are mesoporous materials. The mesoporosity of AC/TiO<sub>2</sub> was significantly reduced when the microwave power was increased to 900 W, which could be due to the destroyed AC pores.

According to IUPAC classification, the N<sub>2</sub> adsorption isotherms of the samples are essentially of type IV with a type-H<sub>4</sub> hysteresis loop (Fig. 2). This characteristic indicates that synthesized materials present mesoporous structure with slit-shaped pores, which is similar to the result obtained by Pastravanu et al. [29]. In the mesoporous carbon sample, AC/TiO<sub>2</sub> exhibited almost the same shape with a small difference in N<sub>2</sub> adsorbed volume. This characteristic is an indication of carbon mesopore filling with titania nanoparticles that resulted in reduced SBET (Table 1). However, during TiO<sub>2</sub> deposition, the hysteresis shape tended toward an H<sub>2</sub>-type, suggesting the evolution of slit-shape into a complex pore structure. All isotherms showed a significant hysteresis at the relative pressure  $P/P_0$  between 0.05 and 0.2, which indicates the existence of mesoporosity in the nanospheric samples [1].

Table 1 The characterization results of different samples

Samples	SBET <sup>a</sup> (m <sup>2</sup> /g)	V <sub>t</sub> <sup>b</sup> (cm <sup>3</sup> /g)	d <sub>pore</sub> <sup>c</sup> (nm)	D <sub>hkl</sub> <sup>d</sup> (nm)	d <sub>particle</sub> <sup>e</sup> (nm)	A/R <sup>f</sup>	M <sup>g</sup> (%)
AC	1915	1.020	3.829	/	/	/	/
AC/TiO <sub>2</sub> -100W	332	0.196	3.414	11.6	12	A	30.81
AC/TiO <sub>2</sub> -300W	364	0.215	3.828	22.6/24.5	30	34/66	42.97
AC/TiO <sub>2</sub> -500W	498	0.237	3.825	46.8/49.3	45	39/61	52.56
AC/TiO <sub>2</sub> -700W	547	0.362	3.828	17.9/22.9	17	47/53	58.72
AC/TiO <sub>2</sub> -900W	190	0.121	3.829	48.3/50.2	45	78/22	47.51

a BET specific surface area.

b Total pore volume taken at  $P/P_0 = 0.98$ .

c Mean pore diameter calculated with BJH method.

d Crystallite size of anatase and rutile calculated with Scherrer equation.

e Mean particle size of TiO<sub>2</sub> determined from TEM.

f Phase ratio of anatase and rutile.

g Percentage composition of TiO<sub>2</sub> calculated by ash method

Adsorbed volume, cc/g STP

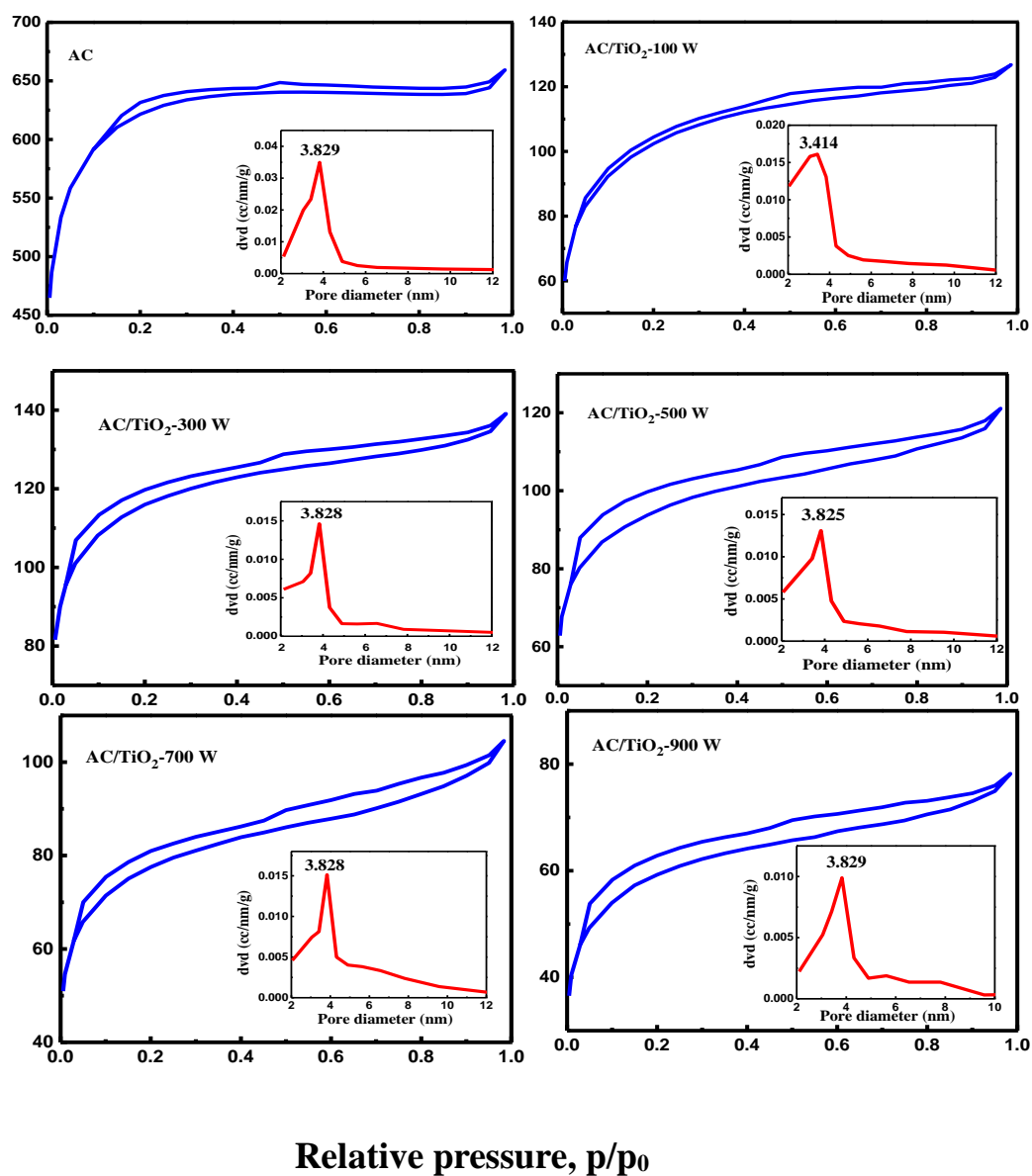


Fig. 2 Nitrogen adsorption-desorption BET isotherms and pore size distribution curves (inset) of AC and AC/TiO<sub>2</sub>.

### 3.3 SEM

The morphology of the synthesized samples was examined through SEM, and the typical SEM micrographs of AC, TiO<sub>2</sub>, and AC/TiO<sub>2</sub> are shown in Fig. 3. The uncoated AC particle surface was smooth. By contrast, for AC/TiO<sub>2</sub>, TiO<sub>2</sub> particles were distributed on the AC surface and no significant changes in the internal morphology of AC were observed as shown in the SEM

199 micrographs (Fig. 3 (a)–(e)). Changing the microwave power resulted in different distributions and  
200 covered areas of TiO<sub>2</sub> on the AC surface, although a portion on the AC surface remained  
201 unoccupied as shown in the lower magnification micrograph on the left side of Fig. 3; this finding  
202 is consistent with BET results. The high-magnification images on the right side of Fig. 3 indicate  
203 that the synthesized TiO<sub>2</sub> features 20 to 50 nm size and a spherical shape. When the microwave  
204 power was increased from 100 to 700 W, more TiO<sub>2</sub> particles formed on the AC surface. Under  
205 microwave preparation conditions of 700 W for 15 min, photocatalytic particles were relatively  
206 uniform, spherical in shape, and better dispersed on AC. And compared with TiO<sub>2</sub>, the coated-TiO<sub>2</sub>  
207 particles become pronounced and coarse by pitch treatment and the size of the particles is kept  
208 large. While the microwave power rising to 900 W, the TiO<sub>2</sub> particle was highly agglomerated due  
209 to the low stability of the small-sized particles, and leading to the TiO<sub>2</sub> gather on the surface of  
210 AC.

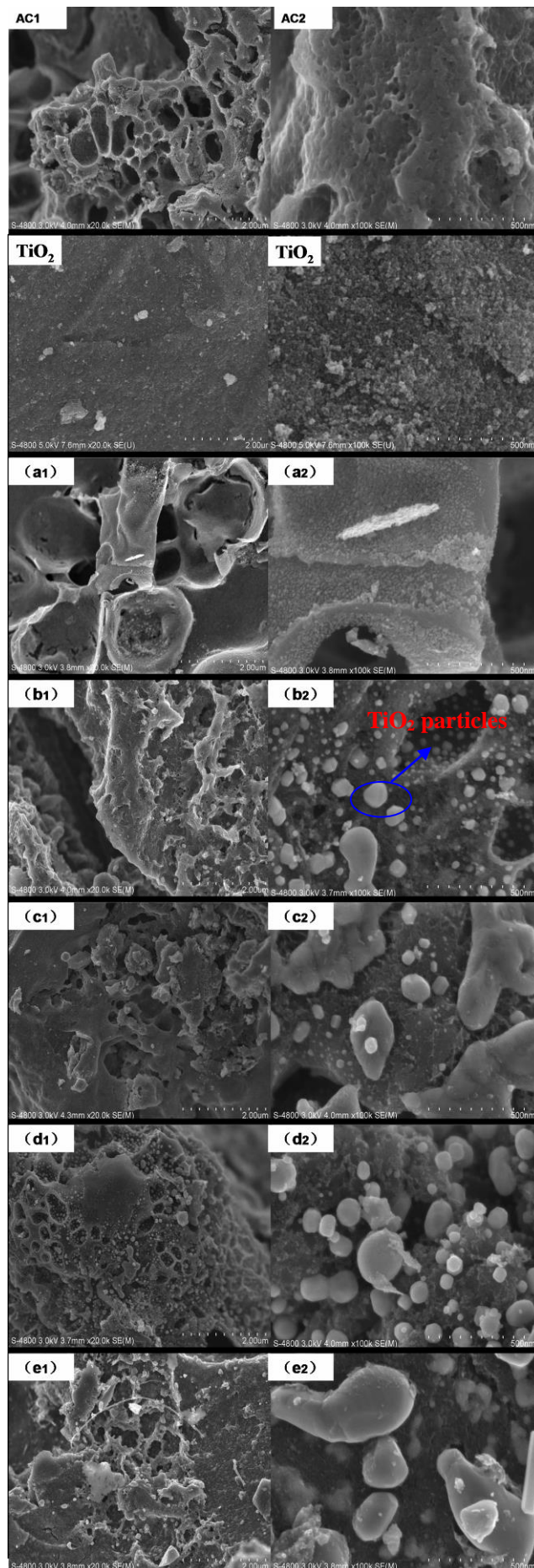


Fig. 3 SEM of AC, TiO<sub>2</sub> and AC/TiO<sub>2</sub>: (a) AC/TiO<sub>2</sub>-100 W, (b) AC/TiO<sub>2</sub>-300 W, (c) AC/TiO<sub>2</sub>-500 W, (d) AC/TiO<sub>2</sub>-700 W, (e) AC/TiO<sub>2</sub>-900 W.

### 3.4 TEM

Fig. 4 shows the TEM micrographs of AC/TiO<sub>2</sub> samples recorded under different magnifications. Under low magnification, the TEM micrograph showed spherical TiO<sub>2</sub> particles distributed on the AC surface, which was also observed in the SEM measurements. Under high magnification, the particle sizes (nm) of the spherical-shaped TiO<sub>2</sub> crystals are distributed as follows: (a) 10–15 nm, (b) 20–50 nm, (c) 40–50 nm, (d) 15–20 nm, and (e) 40–50 nm; these findings are consistent with the XRD results. Only a small amount of TiO<sub>2</sub> particles formed on the AC surface at a microwave power of 100 W for 30 min, and the particle size of TiO<sub>2</sub> is very small with an unstable morphology and structure. Thus, a very low microwave power is not conducive to the formation of the TiO<sub>2</sub> core-shell structure. The amount of TiO<sub>2</sub> particles loaded on AC increased when the microwave power increased from 100 to 700 W (Table 1). The images showed that TiO<sub>2</sub> nanoparticles are uniform in size and shape, free from aggregation, and well-dispersed on AC when the preparation power was 700 W. However, when the microwave power was increased to 900 W, TiO<sub>2</sub> spheres with close interconnection showed serious agglomeration. Thus, the AC/TiO<sub>2</sub>-700 W photocatalyst could provide the free surface of AC for dye adsorption on the microspheres, and the transfer of the dye around TiO<sub>2</sub> resulted in enhanced dye degradation.



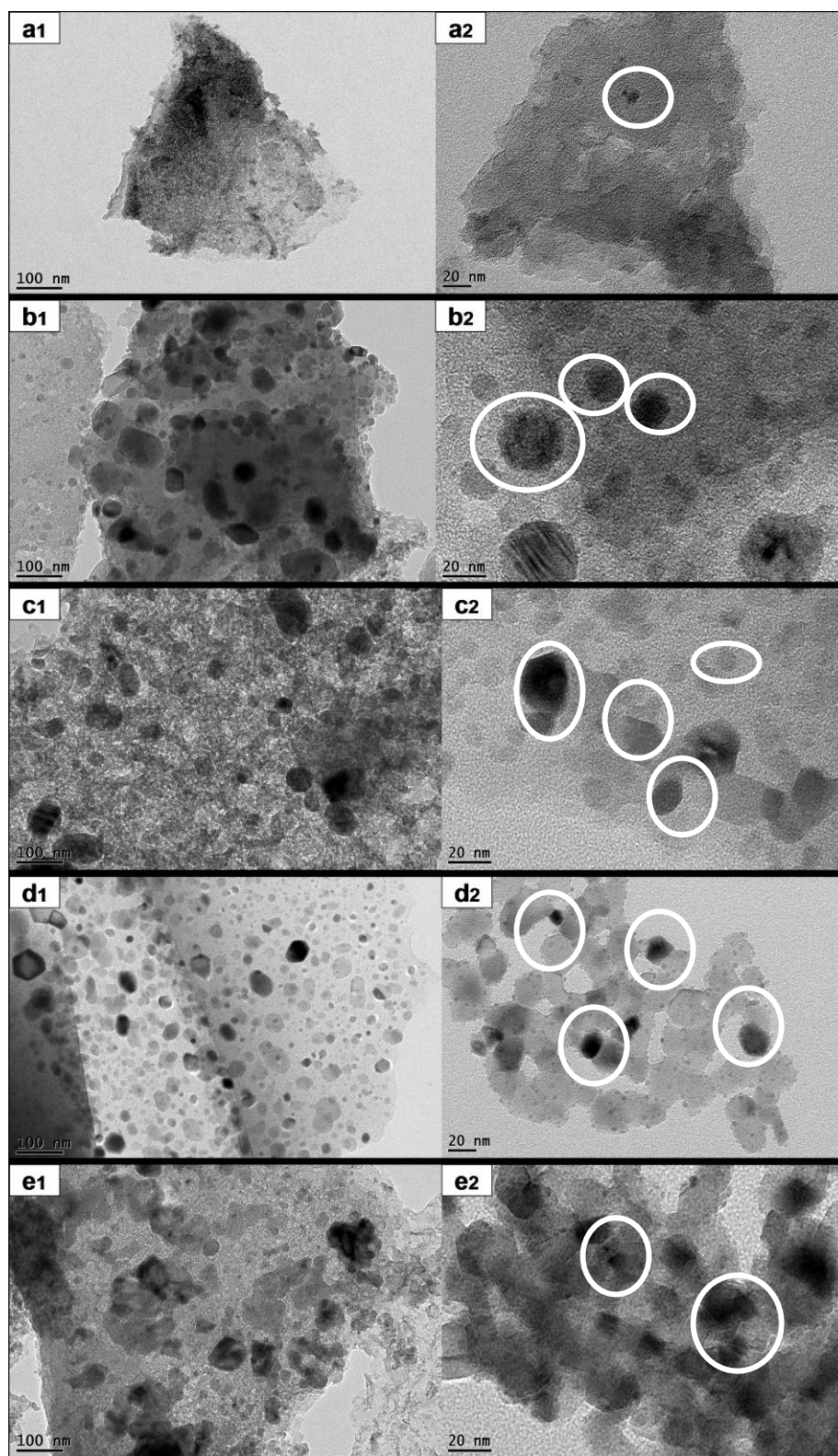


Fig. 4 TEM of AC/TiO<sub>2</sub>: (a) AC/TiO<sub>2</sub>-100 W, (b) AC/TiO<sub>2</sub>-300 W, (c) AC/TiO<sub>2</sub>-500 W, (d) AC/TiO<sub>2</sub>-700 W, (e) AC/TiO<sub>2</sub>-900 W.

### 3.5 FTIR

We performed FTIR experiments to determine the surface activity of the catalysts. [Fig. 5](#)



shows the FTIR spectra of AC and AC/TiO<sub>2</sub> nanocomposites in the spectral region from 450 to 4000 cm<sup>-1</sup>. The strong peak of the AC/TiO<sub>2</sub> nanocomposites around 3425 and 2360 cm<sup>-1</sup> are attributed to asymmetric stretching vibration of O–H, which are similar to those of the AC samples. This finding indicates that no dehydroxylation occurred during formation of AC/TiO<sub>2</sub> nanocomposites. The improved hydrophilicity and wettability of the mesoporous carbon are advantageous for organic adsorption from aqueous solutions [28]. The main reason for this benefit may be that the very short heating time and the activity of rapid resolidification of molten phases, in conjunction with the aqueous environment, avoids the dehydroxylation of AC. The comparison of the curves of AC and AC/TiO<sub>2</sub> and FTIR results suggest that the formation of titania nanoparticles in the AC/TiO<sub>2</sub> nanocomposites did not alter the structure or phase of the AC crystals. The broad absorption band in the range of 400–800 cm<sup>-1</sup> characterizes the Ti–O and Ti–O–Ti vibration of anatase, which confirms the formation of TiO<sub>2</sub>. Moreover, the appearance of bands at 1080 cm<sup>-1</sup> indicates the clear formation of the Ti–O–C bonds, suggesting that TiO<sub>2</sub> binds to the mesoporous carbon surface [29].

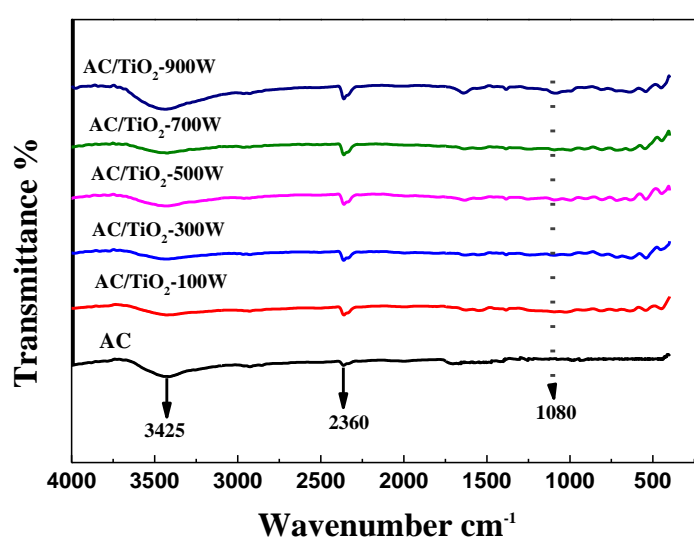


Fig. 5 FTIR spectra of AC and AC/TiO<sub>2</sub>: (a) AC/TiO<sub>2</sub>-100 W, (b) AC/TiO<sub>2</sub>-300 W, (c) AC/TiO<sub>2</sub>-500 W, (d) AC/TiO<sub>2</sub>-700 W, (e) AC/TiO<sub>2</sub>-900 W.

### 3.6 XPS

To understand the oxidation states of Ti, we conducted XPS measurements of TiO<sub>2</sub> (prepared for 700 W with 15 min) and AC/TiO<sub>2</sub>-700 W (Fig. 6). Ti 2p 1/2 and Ti 2p 3/2 peaks were observed in pure TiO<sub>2</sub>, with binding energies of 465.3 and 459.75 eV, respectively, and the binding energies of these peaks in the AC/TiO<sub>2</sub> samples shifted toward 465.2 and 459.5 eV, respectively. The observed range of the 2p binding energy values for TiO<sub>2</sub> and AC/TiO<sub>2</sub> samples indicates that Ti is in the +4 oxidation state [28]. Therefore, Ti in the AC/TiO<sub>2</sub> nanocomposites is the TiO<sub>2</sub> derived from titania. The XPS results confirmed the formation of titania in the AC/TiO<sub>2</sub> nanocomposites and indicated the stability of the TiO<sub>2</sub> nanocomposite under the reaction condition.

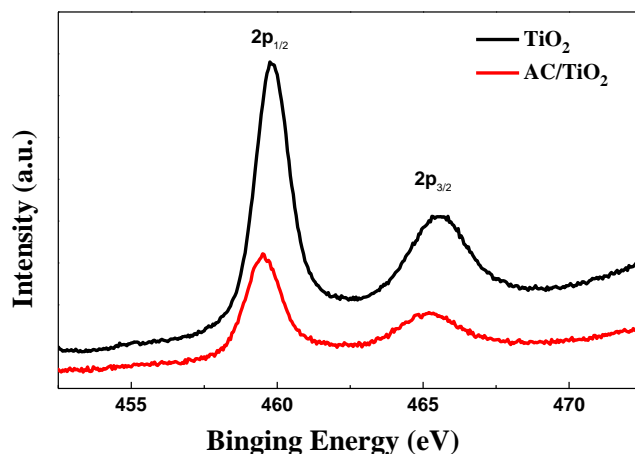


Fig. 6 XPS of Ti 2p in TiO<sub>2</sub> and AC/TiO<sub>2</sub>-700 W.

### 3.7 UV-vis spectra

The UV-vis DRS of TiO<sub>2</sub> (prepared for 700 W with 15 min) and AC/TiO<sub>2</sub> samples are shown in the inset Fig. 7. With TiO<sub>2</sub> loaded on AC, the absorbance in the visible region was enhanced. Pure TiO<sub>2</sub> showed an intrinsic absorption with light wavelength shorter than 390 nm and almost no absorption in visible light with wavelength ranging from 400 to 800 nm. This adsorption is mainly attributed to the inter-band transition of TiO<sub>2</sub> [11]. The light absorption edge of

AC/TiO<sub>2</sub>-700 W was 412 nm, with a remarkable red shift to the visible range compared with the spectrum of pure TiO<sub>2</sub>. This change influenced the effective band gap of the photocatalyst. TiO<sub>2</sub> is known as an indirect semiconductor, for which the relation between absorption coefficient ( $\alpha$ ) and the incident photon energy ( $h\nu$ ) can be written as  $\alpha=B_i (h\nu-E_g)^2/h\nu$  [3], where  $B_i$  is the absorption constant for indirect transitions. Plots of  $(\alpha h\nu)^{1/2}$  versus  $h\nu$  from the spectral data are presented of Fig. 7. Thus, the sample AC/TiO<sub>2</sub> was found to have band gap 2.67 eV which was lower than the band gap of the initial titania powder (2.91 eV) and for this reason it is expected the AC-TiO<sub>2</sub> to be photocatalytically active under visible light. Moreover, Zhang [15] reported that absorbance in the presence of AC/TiO<sub>2</sub> was higher than that in the presence of AC.

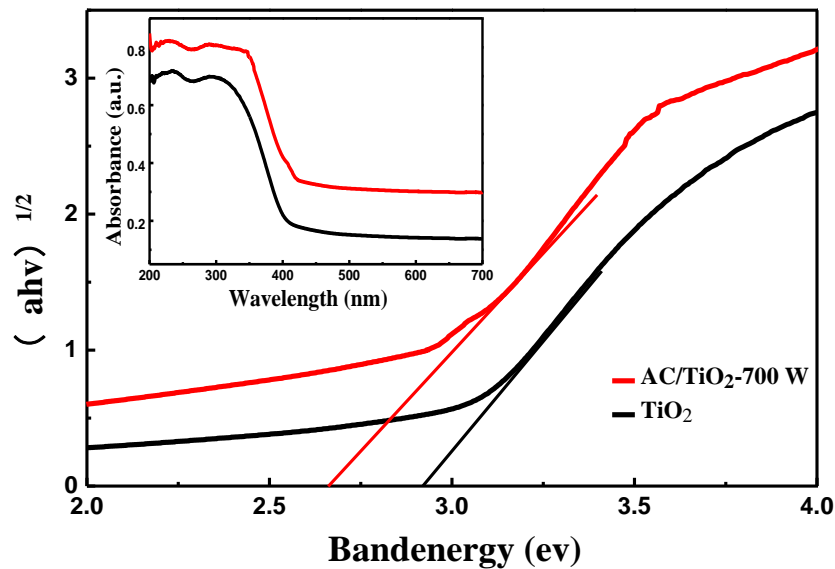


Fig. 7 Diffuse reflectance absorption spectra of TiO<sub>2</sub> and AC/TiO<sub>2</sub>-700 W.

### 3.8 Photocatalytic activity

The activities of the synthesized nanocomposites were evaluated through photodegradation of RhB aqueous solution (30 mg/L) under UV irradiation at 365 nm (Fig. 8). A blank experiment without any photocatalyst (photolysis) was conducted for comparison. No evident photodegradation of RhB was observed after 30 min of irradiation in the absence of photocatalyst

(direct photolysis). The pure photolytic removal efficiency of the as-synthesized TiO<sub>2</sub> sample (for 700 W with 15 min) was 18.52%, and the adsorption efficiency of AC was 20%, exclusive of the 30 min dark reaction. The removal efficiency of AC/TiO<sub>2</sub> composite samples presented high photolytic removal efficiency that ranged from 37 to 95% (Fig. 8 (inset)). TiO<sub>2</sub> loaded on AC exhibited very high photocatalytic degradation efficiency compared with AC and pure TiO<sub>2</sub>. The substantially decrease in RhB concentration in the aqueous solution can occur in a physical–chemical phenomenon, such as adsorption by AC and photocatalytic decomposition by TiO<sub>2</sub>. The activated carbon played a role of adsorption at the ratio 1:10 (AC and TiO<sub>2</sub>-sel), and most channel of active carbon was not dominated by the titanium dioxide [31]. The mesoporous carbon with appropriate content may contribute to RhB molecules gather around TiO<sub>2</sub> particles in low concentration solution of RhB, which improve the photocatalytic degradation process. Therefore, the role of carbon pore structures is very important, which facilitate the diffusion of RhB reactants and products on the TiO<sub>2</sub> active sites during the photocatalytic reaction. Similarly, Pastravanu et al. [29] reported that even after 170 min of irradiation time, 92% MO was degraded when the sample prepared through 7 min of microwave radiation was used as the photocatalyst; nevertheless, only 42% of dye conversion was achieved in the case of pure TiO<sub>2</sub>. The RhB removal efficiencies followed the order of AC/TiO<sub>2</sub>-700 W > AC/TiO<sub>2</sub>-500 W > AC/TiO<sub>2</sub>-300 W > AC/TiO<sub>2</sub>-900 W > AC/TiO<sub>2</sub>-100 W. Nearly complete RhB photodegradation was further observed when the microwave power was 700 W.

In a microwave oven, heat is generated from within the sample through the interaction of microwaves with microwave-susceptible materials [25]. Therefore, the AC core was expected to first interact with the microwaves to generate heat that will be transmitted to the TiO<sub>2</sub> shell,

resulting in the formation of the anatase phase (Fig. 1) at a relatively low power of 100 W. When the microwave power exceeded 100 W, the phase of rutile gradually formed. Many studies reported that the mixed-phase TiO<sub>2</sub> (anatase and rutile) exhibits higher photocatalytic activity than the pure phase because of the charge trapping and transfer at the phase interfaces of the mixed TiO<sub>2</sub> [5, 17, 23]. The anatase/rutile ratio is a more important factor in determining the photocatalytic activity of the prepared AC/TiO<sub>2</sub> through the formation of ·OH [21, 32]. With the increase of microwave power, the ratio of anatase/rutile decreased see in Table 1. When the power increased to 700 W, the ratio of anatase/rutile was 47/53, which was beneficial to the formation of ·OH. Lv et al. [22] reported the highest ·OH formation rate was observed when the two phase structures of anatase and rutile phases with a ratio of 57:43. Moreover, all the AC/TiO<sub>2</sub> composites exhibited higher PL intensity than pure TiO<sub>2</sub>, suggesting that loading of TiO<sub>2</sub> on the surface of AC was a good route to induce the transfer and separation of the photogenerated charge carriers, which resulted in the increase of ·OH formation (Fig. 9). The following order was the generation rate of ·OH radicals of the catalysts: AC/TiO<sub>2</sub>-700 W > AC/TiO<sub>2</sub>-500 W > AC/TiO<sub>2</sub>-300 W AC/TiO<sub>2</sub>-900 W > AC/TiO<sub>2</sub>-100 W > TiO<sub>2</sub>. The result is in accordance with the photocatalytic activities of the photocatalysts in Fig. 8. So, the photocatalytic activity of the photocatalysts could be contributed to amounts of ·OH induced in the reaction system to some extent. The degradation mechanism for the AC/TiO<sub>2</sub> was similarly with the reported by Xiang et al. [23] that the activity of photocatalysts depending on the ·OH. In addition, surface area is another important factor in determining the photocatalytic activity of the prepared AC/TiO<sub>2</sub>. The AC/TiO<sub>2</sub>-100 W sample remained mostly amorphous TiO<sub>2</sub> which covered on the surface of AC because the maximum temperature reached was low with 30 min radiation. The amount of stable TiO<sub>2</sub> produced increased when the

microwave power was increased from 300 to 700 W, which resulted in an increase in TiO<sub>2</sub> loading on AC (Table 1). The rest of the amorphous TiO<sub>2</sub> detached from AC, thus increasing the exposed area of the carbon. Therefore, the photocatalytic effect of particles increased with increasing microwave power as evidenced by the synergistic relationship between AC and TiO<sub>2</sub>. When the microwave power was increased to 900 W, the SBET significantly decreased because the high temperature induced TiO<sub>2</sub> agglomeration as shown in Fig. 3, resulting in decreased photolysis efficiency.

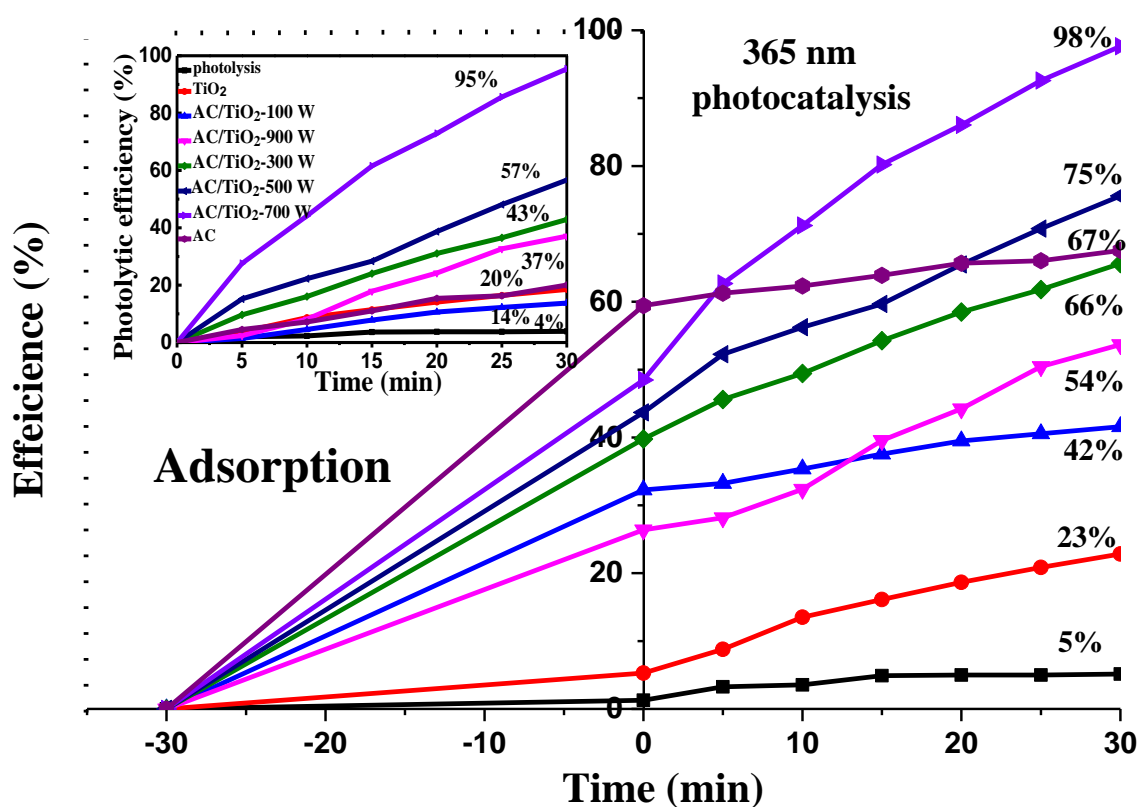


Fig. 8 RhB remove efficiencies over catalysts under 365 nm UV light (RhB concentration of 30 mg/L).

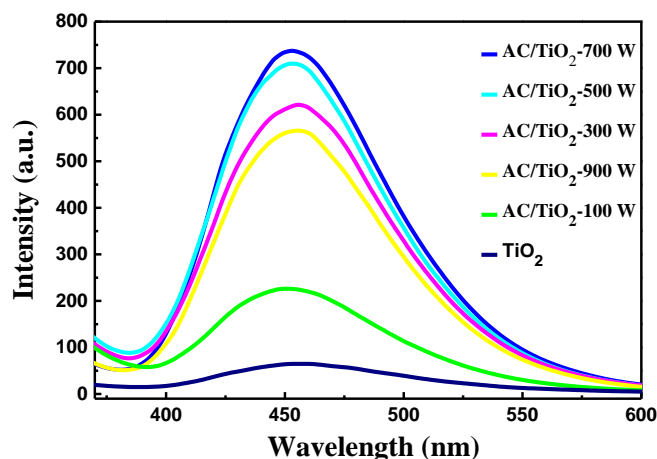
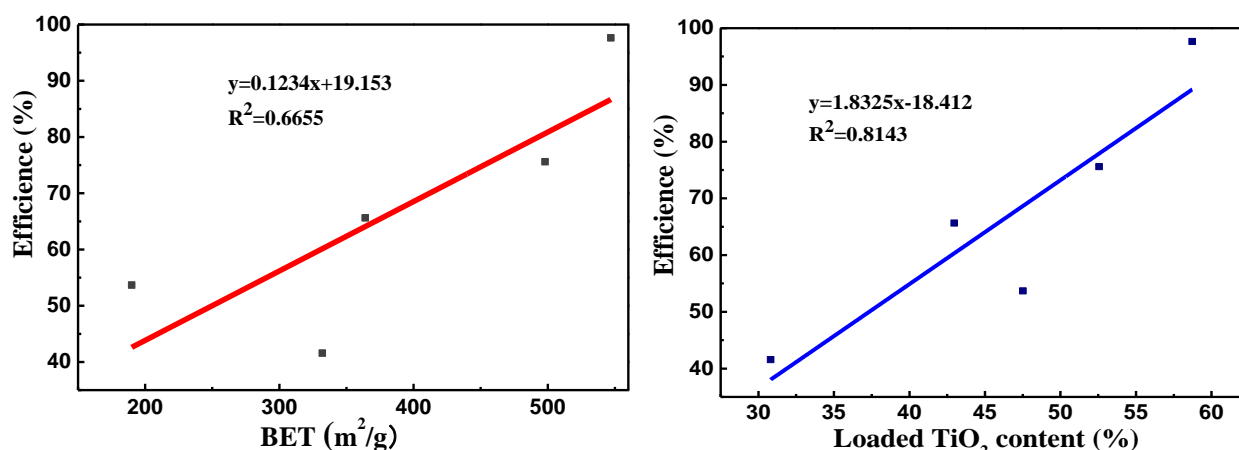


Fig. 9 PL spectra of pure TiO<sub>2</sub> and AC/TiO<sub>2</sub> prepared by different microwave conditions

### 3.9 Correlation analysis

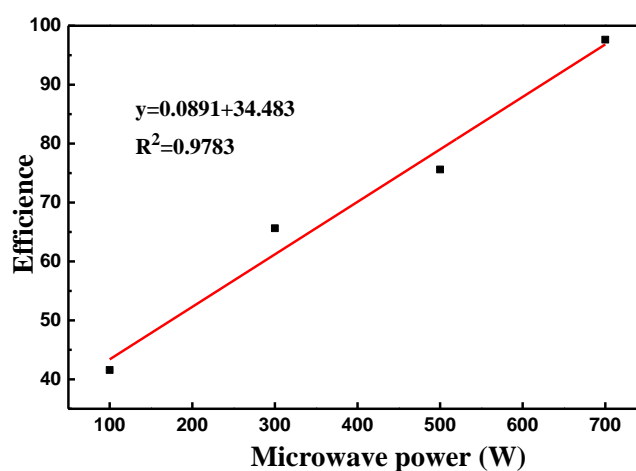
The photocatalytic reaction process is complex and affected by several factors, such as TiO<sub>2</sub> content, morphology, and SBET. Correlation analysis was further conducted to study the effect of each factor on RhB removal efficiency. Fig. 10 shows that SBET and percentage composition of TiO<sub>2</sub> presented a good linear relationship to RhB removal efficiency in the tested AC/TiO<sub>2</sub> ( $R^2=0.6655$  and  $R^2=0.8143$ ). A high surface area of AC/TiO<sub>2</sub> with more TiO<sub>2</sub> content will generally result in high removal efficiency. Previous study showed that AC and TiO<sub>2</sub> has a synergetic effect on the photocatalytic RhB degradation, which could be ascribed to the enhanced adsorption of the pollutants on AC, followed by transfer from the interphase to titania, where the pollutants were photodegraded [19]. On the one hand, a large portion of the AC surface remained unoccupied, which shows that AC/TiO<sub>2</sub> still has very strong adsorptive capacity. Large SBET of the samples may dramatically enlarge the effective reaction surface areas between the photocatalysts and pollutants [5]. On the other hand, increased TiO<sub>2</sub> content could rapidly degrade RhB under irradiation. In addition, the correlation of microwave power (100-700 W) and removal efficiency has been shown in Fig.10 (c), which closed to the linear. So the AC/TiO<sub>2</sub>-700 W sample was considered to own the highest photocatalytic activity, which was mainly attributed to the high

sorption properties of mesoporous carbon material and high amount of TiO<sub>2</sub>. Thus, the surface area and TiO<sub>2</sub> content of AC/TiO<sub>2</sub> should be as high as possible to improve AC/TiO<sub>2</sub> performance for RhB photocatalytic degradation.



(a)

(b)



(c)

Fig.10. (a) BET surface area and remove efficiency of RhB (b) loaded TiO<sub>2</sub> content and remove efficiency of RhB (c) microwave power (100-700 W) and remove efficiency of RhB

## 4. Conclusions

In this study, AC/TiO<sub>2</sub> nanocomposites were efficiently prepared using microwave radiation technology. The proposed method features simplicity, flexibility, short reaction times, and high photocatalytic efficiency. XRD analysis confirmed that TiO<sub>2</sub> nanoparticles are anatase and rutile



with a particle size of 20–50 nm. The SEM and TEM analyses indicated that TiO<sub>2</sub> nanoparticles are spherical in shape and well distributed on the AC surface. The SBETs of the AC/TiO<sub>2</sub> composites decreased with increasing TiO<sub>2</sub> loading, but a large portion of the AC surface remained unoccupied. From the UV-vis spectrum, an obvious red-shift was observed when TiO<sub>2</sub> coated the AC surface. The efficiency of the samples followed the order: AC/TiO<sub>2</sub>-700 W > AC/TiO<sub>2</sub>-500 W > AC/TiO<sub>2</sub>-300 W > AC/TiO<sub>2</sub>-900 W > AC/TiO<sub>2</sub>-100 W > TiO<sub>2</sub>, which was related to the formation rate of ·OH. For AC/TiO<sub>2</sub>-700 W, the removal efficiency of RhB reached to 98% after 30 min of UV irradiation. The high surface area with high TiO<sub>2</sub> content of AC/TiO<sub>2</sub> showed good RhB photocatalytic degradation. The proposed method for preparation of photocatalysts with improved structural features and excellent photocatalytic effect can be easily implemented and is economical, and the resulting composite can be potentially applied in water pollution treatment.

## Acknowledgements

This work was supported financially by funding from the National Natural Science Foundation of China (51262025), International scientific and technological cooperation project of Xinjiang Bingtuan (2013BC002) and Graduate Research Innovation Project in Xinjiang (XJGRI2014053).

## References

- [1] N. Guo, Y.M. Liang, S. Lan, L. Liu, G.J. Ji, S.C. Gan, H.F. Zou, X.C. Xu, Uniform TiO<sub>2</sub>-SiO<sub>2</sub> hollow nanospheres: synthesis, characterization and enhanced adsorption–photodegradation of azo dyes and phenol, *Appl. Surf. Sci.* 305 (2014) 562-574.
- [2] S.F. Chen, Y.F. Hu, S.G. Meng, X.L. Fu, Study on the separation mechanisms of photogenerated electrons and holes for composite photocatalysts g-C<sub>3</sub>N<sub>4</sub>-WO<sub>3</sub>, *Appl. Catal. B-Environ.* 150-151 (2014) 564-573.

- [3] N. Todorova, T. Giannakopoulou, S. Karapati, D. Petridis, T. Vaimakis, C. Trapalis, Composite TiO<sub>2</sub>/clays materials for photocatalytic NO<sub>x</sub> oxidation, *Appl. Surf. Sci.* 319 (2014) 113-120.
- [4] L. Gomathi Devi, S. Girish Kumar, B. Narasimha Murthy, Nagaraju Kottam, Influence of Mn<sup>2+</sup> and Mo<sup>6+</sup> dopants on the phase transformations of TiO<sub>2</sub> lattice and its photo catalytic activity under solar illumination., *Catal. Commun.* 10 (2009) 794-798.
- [5] S. Photong, V. Boonamnuyvitaya, Preparation and characterization of amine-functionalized SiO<sub>2</sub>/TiO<sub>2</sub> films for formaldehyde degradation, *Appl. Surf. Sci.* 255 (2009) 9311-9315.
- [6] W.J. Liang, J. Li, Y.Q. Jin, Photo-catalytic degradation of gaseous formaldehyde by TiO<sub>2</sub>/UV, Ag/TiO<sub>2</sub>/UV and Ce/TiO<sub>2</sub>/UV, *Build. Environ.* 51 (2012) 345-350.
- [7] Z. Ma, Cobalt oxide catalysts for environmental remediation, *Current Catalysis* 3 (2014) 15-26.
- [8] D.G. Calatayud, T. Jardiel, M. Peiteado, A.C. Caballero, D. Fernández-Hevia, Microwave-induced fast crystallization of amorphous hierarchical anatase microspheres, *Nanoscale Res. Lett.* 9 (2014) 273-278.
- [9] S. Girish Kumar, K.S.R. Koteswara Rao, Zinc oxide based photocatalysis: tailoring surface-bulk structure and related interfacial charge carrier dynamics for better environmental applications, *RSC Adv.* 5 (2015) 3306-3351.
- [10] L. Gomathi Devi, R. Kavitha, Review on modified N-TiO<sub>2</sub> for green energy applications under UV/visible light: selected results and reaction mechanisms, *RSC Adv.* 4 (2014) 28265-28299.
- [11] L.F. Chiang, R. Doong, Cu-TiO<sub>2</sub> nanorods with enhanced ultraviolet- and visible-light photoactivity for bisphenol A degradation, *J. Hazard. Mater.* 277 (2014) 84-92.
- [12] S.G. Liu, J.G. Yu, B. Cheng, M. Jaroniec, Fluorinated semiconductor photocatalysts: Tunable synthesis and unique properties, *Adv. Colloid Interfac.* 173 (2012) 35-53.
- [13] L. Gomathi Devi, R. Kavitha, A review on non metal ion doped titania for the photocatalytic degradation of organic pollutants under UV/solar light: Role of photogenerated charge carrier dynamics in enhancing the activity, *Appl. Catal. B-Environ.* 140-141 (2013) 559-587.
- [14] S. Girish Kumar, L. Gomathi Devi, Review on modified TiO<sub>2</sub> photocatalysis under UV/visible light: selected results and related mechanisms on interfacial charge carrier transfer dynamics, *J. Phys. Chem. A* 115 (2011) 13211-13241.
- [15] Z. Zhang, Y. Xu, X. Ma, F. Li, D. Liu, Z. Chen, F. Zhang, D.D. Dionysiou, Microwave degradation of methyl orange dye in aqueous solution in the presence of nano-TiO<sub>2</sub>-supported activated carbon (supported-TiO<sub>2</sub>/AC/MW). *J. Hazard. Mater.* 209-210 (2012) 271-277.
- [16] J.G. Yu, M. Jaroniec, Photocatalytic materials for energy and environmental applications, *Appl. Surf. Sci.* 319 (2014) 136-142.
- [17] F. Teng, G.Z. Zhang, Y.Q. Wang, C.T. Gao, L.L. Chen, P. Zhang, Z.X. Zhang, E.Q. Xie, The role of carbon in the photocatalytic reaction of carbon/TiO<sub>2</sub> photocatalysts, *Appl. Surf. Sci.* 320 (2014) 703-709.
- [18] G.H. Li, K.A. Gray, The solid-solid interface: Explaining the high and unique photocatalytic reactivity of TiO<sub>2</sub>-based nanocomposite materials, *Chem. Phys.* 339 (2007) 173-187.
- [19] S. Girish Kumar, K.S.R. Koteswara Rao, Polymorphic phase transition among the titania crystal structures using a solution-based approach: from precursor chemistry to nucleation process, *Nanoscale* 6 (2014) 11574-11632.
- [20] M.L. Chen, J.S. Bae, W.Ch. Oh, Characterization of AC/TiO<sub>2</sub> composite prepared with pitch binder and their photocatalytic activity, *B. Kor. Chem. Soc.* 27 (2006) 1423-1228.

- [21] H. Xu, L.Z. Zhang, Controllable one-pot synthesis and enhanced photocatalytic activity of mixed-phase TiO<sub>2</sub> nanocrystals with tunable brookite/rutile ratios, *J. Phys. Chem. C*, 113 (2009) 1785-1790.
- [22] K. Lv, J.G. Yu, K.J. Deng, X.H. Li, M. Li, Effect of phase structures on the formation rate of hydroxyl radicals on the surface of TiO<sub>2</sub>. *J. Phys. Chem. Solids* 71 (2010) 519-522.
- [23] Q.J. Xiang, J.G. Yu, Quantitative characterization of hydroxyl radicals produced by various photocatalysts, *J. Colloid Interf. Sci.* 357 (2011) 163-167.
- [24] X.M. Xiao, F. Tian, Y.J. Yan, Z.S. Wu, Adsorption behavior of pyrene from onto coal-based activated carbons prepared by microwave activation, *J. Shihezi Univ.* 32 (2014) 485-490.
- [25] Y. Wang, J.G. Yu, W. Xiao, Q. Li, Microwave-assisted hydrothermal synthesis of graphene based Au-TiO<sub>2</sub> photocatalysts for efficient visible-light hydrogen production, *J. Mater. Chem. A* 2 (2014) 3847-3855.
- [26] P. Chen, J.D. Peng, C.H. Liao, P.S. Shen, P.L. Kuo, Microwave-assisted hydrothermal synthesis of TiO<sub>2</sub> spheres with efficient photovoltaic performance for dye-sensitized solar cells, *J. Nanopart. Res.* 15 (2013) 1465-1476.
- [27] K.-i. Ishibashi, A. Fujishima, T. Watanabe, K. Hashimoto, Detection of active oxidative species in TiO<sub>2</sub> photocatalysis using the fluorescence technique, *Electrochem. Commun.* 2 (2000) 207-210.
- [28] J.C. Sin, S.M. Lam, I. Satoshi, K.T. Lee, A.R. Mohamed, Sunlight photocatalytic activity enhancement and mechanism of novel europium-doped ZnO hierarchical micro/nanospheres for degradation of phenol. *Appl. Catal. B-Environ.* 148-149 (2014) 258-268.
- [29] C. Coromelci-Pastravanu, M. Ignat, E. Popovici, V. Harabagiu, TiO<sub>2</sub>-coated mesoporous carbon: Conventional vs. microwave-annealing process, *J. Hazard. Mater.* 278 (2014) 382-390.
- [30] X.M. Xiao, D.D. Liu, Y.J. Yan, Z. Wu, Z.S. Wu, G. Cravotto, Preparation of activated carbon from Xinjiang region coal by microwave activation and its application in naphthalene, phenanthrene, and pyrene adsorption, *J. Taiwan Inst. Chem. E.* 000 (2015) 1-8.
- [31] F. Tian, Z.S. Wu, Y.J. Yan, X.Y. Ge, Y.B. Tong, Photodegradation of formaldehyde by activated carbon loading TiO<sub>2</sub> synthesized via microwave irradiation, *Korean J. Chem. Eng.* 2015, DOI:10.1007/s11814-014-0338-2.
- [32] L. Gomathi Devi, N. Kottam, S. Girish Kumar, Preparation and characterization of Mn-doped titanates with a bicrystalline framework: Correlation of the crystallite size with the synergistic effect on the photocatalytic activity, *J. Phys. Chem. C* 113 (2009) 15593-15601.